

# Technology Report : Robotic Localization and Navigation System for Visible Light Positioning and SLAM

Weipeng Guan, Babar Hussain, C. Patrick Yue

Department of Electronic and Computer Engineering, The Hong Kong University of Science and Technology, Hong Kong, SAR, China

**Abstract**—Visible light positioning (VLP) technology is a promising technique as it can provide high accuracy positioning based on the existing lighting infrastructure. However, existing approaches often require dense lighting distributions. Additionally, due to complicated indoor environments, it is still challenging to develop a robust VLP. In this work, we proposed loosely-coupled multi-sensor fusion method based on VLP and Simultaneous Localization and Mapping (SLAM), with light detection and ranging (LiDAR), odometry, and rolling shutter camera. Our method can provide accurate and robust robotics localization and navigation in LED-shortage or even outage situations. The efficacy of the proposed scheme is verified by extensive real-time experiment<sup>1</sup>. The results show that our proposed scheme can provide an average accuracy of 2 cm and the average computational time in low-cost embedded platforms is around 50 ms.

**Keywords**—Visible Light positioning (VLP), Mobile Robot, LiDAR-SLAM, Multi Sensors Fusion, High Accuracy, Robust Indoor Positioning

## I. INTRODUCTION

Precise localization is a prerequisite for many autonomous systems, such as robotics, unmanned aerial vehicle, etc. Also, the indoor localization problem is especially challenging, where localization cannot be achieved by GPS due to the satellite signal being greatly attenuated, while the traditional radio based indoor positioning technologies, such as Bluetooth, Wi-Fi, Radio-frequency Identification (RFID) and ultra-wideband (UWB), still have some disadvantages in terms of low accuracy, high latency, electromagnetic interference or high hardware cost [1].

In recent years, localization based on visible light communication (VLC), which is also referred as visible light positioning (VLP), has attracted intensive attentions as it can provide high accuracy positioning based on the existing lighting infrastructure. The modulated LED broadcasts its unique identity (ID) through switching at high frequency imperceptible to the human eye, which can be recognized by photodiodes (PD) [2]-[4] and rolling shutter effect (RSE) camera [5]-[7]. The LED lights can be mapped once for all, as they are normally fixed and not easily vulnerable to environmental changes. Hence, the “last mile problem” of localization is solved via VLP and a priori LED feature map. PD is not an ideal VLP device, since it is sensitive to the light intensity variation and the diffuse reflection of the

light signal, which degrades the positioning accuracy [8]. In contrast, camera-based VLP is favored in both commerce and industry, due to the high positioning accuracy achievable by imaging geometry, and the good compatibility with user devices, such as mobile robots and smartphones. Some state-of-the-art (STOA) VLP systems can offer centimeter-level accuracy on commodity smartphone [9], [10] or mobile robot [5], [11]. Despite the promising performance of existing systems, there remain some practical challenges in VLP.

### A. Motivation

One of most urgent issue arises from the fact that VLP normally require multiple LED observations at a time for successful positioning through trilateration or triangulation. Since normal LED lights offer less usable point features, due to the lack of distinguishable appearance, e.g., one feature for a circular LED [12]. However, the number of decodable LEDs in a camera view is limited by a couple of practical factors, such as deployment density of LEDs and geometry layout, obstruction of the line-of-sight (LOS) views, limited field-of-view (FOV) of the image sensor, the ID-decoding rate cannot maintain 100%, and so on [13]. As such, the shortage or outage of LED can severely deteriorate the performance of camera-only method in reality. To address this problem, different VLP-aided inertial localization methods are proposed [5], [12]-[14], which provide pose estimation by fusing VLP measurements from the camera and the inertial measurement unit (IMU). In [13], An Extended Kalman Filter (EKF)-based loosely-coupled VLP-inertial fusion method is proposed. The presented experimental results demonstrate the functionality that the IMU helps to overcome the moments with lack of VLP coverage. However, IMU would suffer drift over time (cumulative error) or measurement noises (biases). Therefore, these VLP-aided inertial localization methods would suffer from errors during a long-term running. Based on this view, we are motivated to adopt the LiDAR scanning to compensate the accumulated error of the inertial sensor, so that the VLP-aided inertial method can achieve long-term high accurate localization. Additionally, sensors are imperfect, and their measurements are prone to errors. The measurement noise of the VLP, which is caused by fabrication error of the image sensors, is also the bottleneck of the positioning accuracy in the field of image sensor-based VLP [15]. By multi sensors fusion, we can compensate the deficiencies of stand-alone sensors and provide more reliable, more robust

<sup>1</sup> Video Demo Link: <https://www.bilibili.com/video/BV1JX4y137Q7>

estimations.

Simultaneous Localization and Mapping (SLAM) based on LiDAR is useful for building and updating maps within unknown environments, while the robot keeps the information about its location. However, the initial pose for the LiDAR-SLAM is an unsolved problem. Since the SLAM commonly suffer from data sparsity or limited vertical FOV in real-world applications. And how to bootstrap the localization without a relatively accurate manually initial guess has not been well considered [16]. What's more, it is difficult to estimate the pose in environments such as a large space or long corridors without too much variety of observation, since the depth information obtained from the LiDAR rangefinder does not change with time and is considered featureless. In other words, a robot is easy to get lost when the geometry of the environment is quite simple, such as a public space surrounded by a few long walls or circular walls [17]. Therefore, we are motivated to adopt the VLP to provide the pose initialization or calibration for LiDAR-SLAM. We regard the localization problem as a registration problem between local perceptual information from the LiDAR and global coordinate information from the VLP, which can handle the kidnapped problems<sup>2</sup> through the VLP observation to successfully deal with the uncertainty of the initial guess.

Last but not the least, one of the most basic yet important features of intelligent mobile robot are the ability to navigate autonomously [18]. However, to the best of our knowledge, most of the works in the field of VLP only focus on the localization part and ignore the navigation application, which is caused by the lack of the mapping and obstacle detection/avoidance function. The priori LED feature map doesn't include any obstacle information around the environment. Based on this point, we are motivated to adopt the LiDAR-SLAM for map building and obstacle detection, also enhance the robustness localization and navigation for VLP, while the VLP can provide high accurate pose initialization for LiDAR-SLAM.

### B. Contribution

In this work, we proposed loosely-coupled multi-sensor fusion method for VLP and SLAM. Integrating multi-sensor, including RSE-camera, LiDAR, odometry, enables a robot to maximize its perceptual awareness of the environments and obtain sufficient measurements, which is promising for robust indoor localization and navigation. More specifically, to estimate the current pose of the robot and to navigate to the target points, the robot firstly builds map of the previously unknown environment through the LiDAR-SLAM. As for the map building, we develop a VLP-constrained mapping scheme based on LiDAR-SLAM (Gmapping<sup>3</sup>) to construct the occupancy grid map based on the pre-build LED feature map. As for the pose estimation, the multi-sensor localization using VLP, odometry and LiDAR can provide high accuracy indoor localization based on the previously built VLP-constrained map, which is the premise of stable navigation. While the LiDAR is also employed to detect surroundings for obstacle avoidance during the navigation. Additionally, the pose initialization and cumulative error compensation method based on LiDAR scans and VLP fusion is proposed, it takes the advantage of the estimated

location to find the initial orientation of the robot with respect to the previously obtained map. Thus, the crucial problem of the autonomous initialization and localization in robotics is solved.

We highlight the contributions as:

- A VLP-constrained SLAM method based on Gmapping is proposed to align the SLAM map with the prebuilt LED feature map. So that the LiDAR-SLAM localization results can be matched with the VLP output, and the fusion between SLAM and VLP is meaningful.
- Loosely-coupled multi-sensor fusion based on EKF is proposed to achieve high accuracy localization through RSE-camera, LiDAR and odometry. Through the state prediction through odometry motion and measurement update from LiDAR scanner, we can relax the assumption on the minimum number of concurrently observable LEDs required for positioning to zero. Meanwhile, the LiDAR can compensate the cumulative error from the odometry. While the VLP measurement is adopted to provide high accuracy pose initialization or pose calibration when it is available.
- The proposed multi-sensor fusion method for VLP-SLAM scheme is robust to provide autonomous navigation. And it is also lightweight enough to be used on resource-constrained computational platform. It can work with sparse lighting distributions, for a large area of  $12.0 \times 10.8 \times 2.7 \text{ m}^3$ , only 4 LEDs are required to ensure high accurate and reliable pose (refer to position and orientation) estimation.

### C. Organization

The remainder of this paper is organized as follows. Section II introduces the related works. Section III explains the proposed multi-sensor fusion for VLP-SLAM methodology, including the principle of VLP, the SLAM map building based on the VLP-constrained, and the loosely-coupled multi-sensor localization. Section IV presents the experimental evaluation and Section V is the conclusion.

## II. RELATED WORK

### A. RSE Camera-based VLP

As we know, LEDs can transmit data over the air by directly modulating the light intensity at a high frequency which is invisible to human eyes but perceivable by camera or PD. Generally, PD is used as the receiver to capture the signal for the VLC system. Recently, camera based on RSE can be also adopted as the receiver in optical camera communication (OCC) system. The pixels on an RSE-camera are exposed and read out line by line instead of perceiving light at the same time at a single moment. Then the temporally-varying intensity signals from the LED transmitter are mapped to spatially-varying bright or dark strip patterns on the captured image. For a comprehensive understanding of OCC and decoding in RSE camera-based VLP, we refer readers to the works [19]-[22].

Camera-based VLP systems employ modulated LED luminaries mounted at known locations (e.g., the ceiling) as artificial landmarks, associate each LED measurement with the ID coordinate through RSE based OCC, and provide information

<sup>2</sup> [https://en.wikipedia.org/wiki/Kidnapped\\_robot\\_problem](https://en.wikipedia.org/wiki/Kidnapped_robot_problem)

<sup>3</sup> <http://wiki.ros.org/gmapping>



about the camera's relative position and rotation with respect to each detected LED by the LOS and weak perspective projection property. Decimeter/centimeter-level accuracy has been reported in some RSE-camera based VLP systems [6], [7], [10], [15], [23]-[25]. Yet, all these methods treat LED lamps as point sources without geometric information. Thus, multiple known LED anchors are required at a time for trilateration or triangulation. Such approaches rely on dense deployment of LED beacons. To reduce the number of required LEDs in VLP, Ref. [26] no longer treat the captured LED images as a point, but as an image whose geometric features are exploited to determine the receiver's orientation and location relative to the reference LED lamp. However, this method requires additional marker to be placed on the LED. Another straightforward method is to employ angular sensors to measure the receiver's orientation information, thus "compensating" the missing information due to the reduced number of LED lamps. Ref. [27] proposed single LED VLP using image and attitude information from mobile phone to achieve average accuracy of 5.5 cm. Ref. [8] proposed a hybrid positioning algorithm consisting of VLP and pedestrian dead reckoning (PDR) to achieve decimeter-level accuracy. However, the IMU is a local frame with arbitrary yaw at the start of each run, it is not identical to global information which can be directly processed with the VLP, it needs pose initialization. Ref. [12], [14] efficiently relax the assumption on the minimum number of simultaneously observable LEDs from three to one through tightly coupled VLP and IMU localization system. However, they still build up the experimental platform in the area of 5m×4m×2.3m with 23 LEDs, since their system required more than 4 LEDs for initialization. In our previous work [13], we proposed loosely-coupled VLP-inertial fusion scheme, which can relax the requirement of the observable LEDs for positioning to zero. However, the robot has to head along the X-axes of the map before running to obtain the initial orientation. Besides, all of the proprioceptive sensors (IMU, odometry) are subject to cumulative errors when estimating the mobile robot's motion. Therefore, apart from the RSE-camera, another exteroceptive sensors acquire information from the robot's environment, are needed to handle the LED shortage/outage problem and deal with the cumulative errors from the IMU or odometry.

### B. Simultaneous Localization and Mapping

SLAM is essential to a wide range of applications, such as scene reconstruction, robotic exploration, and autonomous driving. It consists in the concurrent construction of a model of the environment (the map), and the estimation of the state of the robot moving within it [28]. SLAM can be divided into two categories according to the sensors: Vision-based SLAM and Laser-based SLAM. Comparing to the other distance measurement devices, the LiDAR sensor makes measurements around itself with a wide scanning angle (2D) and high angular resolution. Besides, as an active sensor, it is invariant to the illumination. The high reliability and precision make the LiDAR sensor a popular option for pose estimation [29]. Cartographer SLAM [30], tinySLAM [31] and FastSLAM [32] has been widely applied for laser range-finder-based mapping and localization. Hector SLAM [33] only use the LiDAR to complete map construction and localization, but high-precision LiDAR is needed. Gmapping SLAM [34] is the most widely used SLAM

package in robotics, which use the Rao-Blackwellized particle filter (RB particle filter) to process the environment perceived by the robot works with the wheel odometry to calculate the robot's position and construct the grid map. This approach has achieved remarkable success and indeed was able to reduce the memory consumption while producing highly accurate grid maps. Therefore, Gmapping is more suitable for low-cost mobile platforms where computational resource is limited. For comprehensive understanding of Gmapping and RB particle filter, the readers are strongly advised to the works [34], [35].

Despite its advantage, the LiDAR sensor is not perfect and with several shortcomings. First of all, the features obtained from the LiDAR is limited, which is caused by the low vertical resolution and the sparse point cloud of it. In addition, although most of the LiDAR offer a horizontal FOV of 360 degrees, it receives only few usable points from the side walls in narrow corridor environment. And the pose estimation based on LiDAR is also easy to get lost when the geometric region of the environment is quite similar. Last but not the least, the rangefinder of the LiDAR is limited, it only receives the local information around the robot, it still cannot perceive the global information of the whole indoor or map environment.

To tackle the problems mentioned above, we proposed the multi-sensor fusion for VLP and SLAM. The VLP can be used to make the robot capable of sensing a wide range of environment through the global information provided by LED beacons. While the observation of external landmarks (LED) is also useful to deduce the trajectory drift of the LiDAR-SLAM and possibly correct it. Thus, combine with VLP, we can achieve more refined, accurate, robust, and global LiDAR-SLAM which meets the intelligent robot application demand.

## III. METHODOLOGY

The proposed multi-sensor fusion for VLP-SLAM aims at enabling sufficiently accurate environment perception (mapping), self-localization, and autonomous navigation, while keeping computational requirements low. To do so, we firstly introduce the single LED VLP with odometry (SLO-VLP). Then the loosely-coupled multi-sensor fusion for VLP-SLAM is introduced to show how to integrate two different exteroceptive sensors (camera and LiDAR) information.

### A. Our SLO-VLP

The time-varying VLP signals from LEDs are perceived by the RSE-camera, as spatially-varying strip patterns. Through the VLP observation, the pose of the robot can be estimated in time. To do so, we need to find its centroid imaging location (also call as region-of-interest, ROI), recognize its identity (LED-ID), and retrieve its 3D position from the registered lights databases (pre-build LED feature map). After that we can obtain the absolute 3D position and azimuth of the robot through SLO-VLP calculation.

#### a) LED-ROI Detection

The RSE-camera can capture barcode-like strip patterns from high-frequency flashing LED during underexposure. Natural features are not observable, while bright objects (e.g., LEDs, background light interference) can be easily distinguished, as shown in Fig.1. We are interested in the image regions that carry VLC information, term as LED-ROI [36]. We firstly binarize the

grayscale image by thresholding, and then dilate the binary image to fill the strip gaps. After that, the match template method is utilized to locate the LED-ROI in the captured image for subsequent VLC decoding. Since only the contour feature information is needed for ROI detection, we do not take every pixel into computation but downsize the captured image with a constant scale, e.g., 6. To avoid the errors caused by down sampling, after the boundary of the LED-ROI is found, all the pixels nearby the obtained LED-ROI would be checked again to detect the precise boundary. Since the number of the pixels in the down-scale image and the double-check pixels are much less than that in the original image, and the proposed way to obtain the LED-ROI template is efficient.

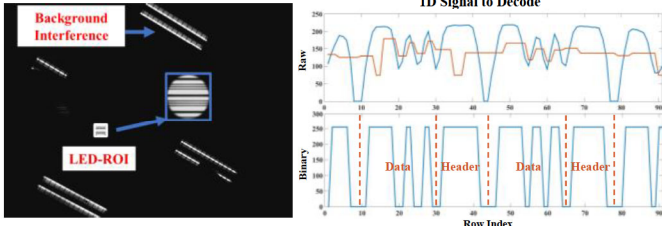


Fig1. Example results for LED-ROI extraction under background light interference (left), and LED-ID decoding (right).

#### b) VLC Coding and Decoding

In this work, we employ our universal VLC modulator [37] for retrofitting LED lamp to transmit the ID information to the RSE-based camera receiver. Each LED lamp is assigned with a unique ID, which is associated with its location and stored in an ID-location database (prebuild LED feature map). The designed ID data packet begins with a 6-bit preamble (header, 011110), proceeded by 8-bit and 8 kHz-frequency OOK-coded data payload data. The payload carries one byte of ID, labeling up to 256 LEDs. The channel capacity is adequate for our experiment implementation and can be extended by a larger packet length. The VLC information is encoded by strips of varying widths. As can be seen in Fig. 1, the grayscale pixels in the centering column of the LED-ROI are selected for OOK demodulation. The thresholding method based on local extremum and sliding window [11] is adopted to counter the nonuniform illumination of LEDs. The decoding rate of our LED-ID decoding method can maintain more than 95% at a height of 2.7m, which had been reported in our previous work [13].

#### c) Single LED VLP with Odometry (SLO-VLP)

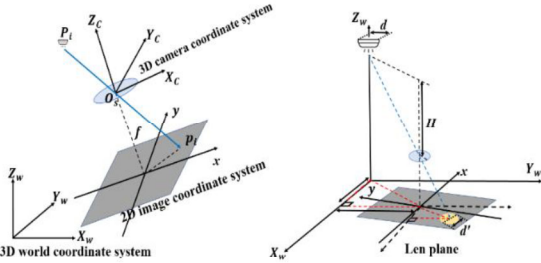


Fig.2 The transforms among the world, camera, and image coordinate systems

Fig.2 shows the schematic diagram of the single LED VLP algorithm, which is based on the pinhole camera model. It involves three coordinate systems: 3-D world coordinate system, 3-D camera coordinate system, and 2-D image plane coordinate system. All of the LEDs  $P_i = [X_i, Y_i, Z_i]^T$  ( $i = 1^{st}, 2^{nd}, \dots, N$ ) in the world coordinate, is mapped onto an image point  $p_i = [x_i, y_i]^T$  ( $i = 1^{st}, 2^{nd}, \dots, N$ ) in the image coordinate through the

lens of the camera ( $i$  is the unique ID). While the  $p_i$  can be measured through the image process pipeline. For any LED  $P_i$  in the world coordinate, we can model the perspective projection model between the world coordinate and the image plane coordinate as:

$$\lambda \begin{bmatrix} x_i \\ y_i \\ 1 \end{bmatrix} = \begin{bmatrix} f/dx & 0 & u_0 & 0 \\ 0 & f/dy & v_0 & 0 \\ 0 & 0 & 1 & 0 \end{bmatrix} \begin{bmatrix} \mathbf{R} & \mathbf{T} \\ \mathbf{0} & 1 \end{bmatrix} \begin{bmatrix} X_i \\ Y_i \\ Z_i \\ 1 \end{bmatrix} \quad (1)$$

Where  $\lambda$  can be represented as the coordinate of the Z axis of LED  $P_i$  in the camera coordinate system,  $f$  is the focal length,  $dx$  and  $dy$  represent the physical size of the pixel,  $\mathbf{T}$  represent the translation vector, which is equivalent to the receiver's position in the 3-D world coordinate system.  $\mathbf{R}$  is the rotation matrix from the 3-D world coordinate system to the 3-D camera coordinate system, as follows:

$$\mathbf{R} = R_x(\alpha) \cdot R_y(\beta) \cdot R_z(\gamma) = \begin{bmatrix} 1 & 0 & 0 \\ 0 & \cos\alpha & \sin\alpha \\ 0 & -\sin\alpha & \cos\alpha \end{bmatrix} \cdot \begin{bmatrix} \cos\beta & 0 & -\sin\beta \\ 0 & 1 & 0 \\ \sin\beta & 0 & \cos\beta \end{bmatrix} \cdot \begin{bmatrix} \cos\gamma & -\sin\gamma & 0 \\ \sin\gamma & \cos\gamma & 0 \\ 0 & 0 & 1 \end{bmatrix} \quad (2)$$

where  $\alpha, \beta$  and  $\gamma$  is the angle along the X, Y, and Z axis. The three rotation angles can be estimated from the proprioceptive sensor (such as IMU or odometry) attached to the robot. Since the robot is moving horizontally on the floor, only the azimuth angle  $\gamma$  is needed to be considered, while the other two rotation angles can be ignored as constant matrix  $\mathbf{C}_\alpha$  and  $\mathbf{C}_\beta$ . Then the Eq. (2) can be expressed as another format:

$$\mathbf{R} = \mathbf{C}_\alpha \cdot \mathbf{C}_\beta \cdot R_z(\gamma) = \mathbf{C}_\alpha \cdot \mathbf{C}_\beta \cdot \begin{bmatrix} \cos\gamma & -\sin\gamma & 0 \\ \sin\gamma & \cos\gamma & 0 \\ 0 & 0 & 1 \end{bmatrix} \quad (3)$$

The pose of the mobile robot moving in 2D plane consists of coordinates and heading orientation, therefore we work with a four-dimensional state vector  $\mathbf{s} = [X_s \ Y_s \ Z_s \ \gamma]^T$ . For the  $Z_s$  of the positioning terminal, it can be calculated by:

$$Z_s = Z_i - H \quad (4)$$

where  $H$  is the vertical distance from center of the camera  $O_s$  to the ceiling, also equal to the  $\lambda$ . The LED image is no longer treated as a point, but as an image whose geometric features are exploited to determine  $Z_s$ . Since the rotation angles along the X and Y axis are taken to  $0^\circ$ , when the robot moves horizontally,  $\mathbf{C}_\alpha$  and  $\mathbf{C}_\beta$  would be the identity matrix. Then vertical distance  $H$  between the LED and the lens plane can be expressed as

$$\frac{H}{f} = \frac{D}{P_d d_{\text{pixel}}} \quad (5)$$

where  $D$  is the physical diameter of the LED,  $d_{\text{pixel}}$  is the pixel distance of the LED-ROI, and  $P_d$  is the conversion of the pixel distance and physical distance. Substituting (4) and (5) into (1), we derive the mathematical relation between the LEDs,  $[X_i, Y_i, Z_i]^T$ , and the observation values of their corresponding imaging points  $[x_i, y_i]^T$ , then we obtain the position of the receiver  $[X_s \ Y_s \ Z_s]$  in the 3-D world coordinate system

$$\frac{fD}{P_d d_{\text{pixel}}} \begin{bmatrix} x_i \\ y_i \\ 1 \end{bmatrix} = \begin{bmatrix} f/dx & 0 & u_0 & 0 \\ 0 & f/dy & v_0 & 0 \\ 0 & 0 & 1 & 0 \end{bmatrix} \begin{bmatrix} \cos\gamma & -\sin\gamma & 0 & X_s \\ \sin\gamma & \cos\gamma & 0 & Y_s \\ 0 & 0 & 1 & Z_s \\ 0 & 0 & 0 & 1 \end{bmatrix} \begin{bmatrix} X_i \\ Y_i \\ Z_i \\ 1 \end{bmatrix} \quad (6)$$



After obtaining the estimation coordinate of the camera's center, the 3D position and azimuth of the robot  $\mathbf{s}_t = [x_t \ y_t \ z_t \ \theta_t]^T$  at time  $t$  can be estimated through the TF transformation<sup>4</sup> as follows:

$$\begin{bmatrix} x_t \\ y_t \\ z_t \\ \theta_t \end{bmatrix} = \mathbf{F}_{tf} \begin{bmatrix} X_s \\ Y_s \\ Z_s \\ \gamma \end{bmatrix} = \begin{bmatrix} r_x & 0 & 0 & 0 \\ 0 & r_y & 0 & 0 \\ 0 & 0 & r_z & 0 \\ 0 & 0 & 0 & 1 \end{bmatrix} \begin{bmatrix} X_s \\ Y_s \\ Z_s \\ \gamma \end{bmatrix} + \begin{bmatrix} t_x \\ t_y \\ t_z \\ 0 \end{bmatrix} \quad (7)$$

where,  $r_x, r_y, r_z$  and  $t_x, t_y, t_z$  are the rotation and translation coefficient from the center of the camera to the base\_link<sup>5</sup> of the robot. However, since the odometry only provides relative motion measurements, the initial pose are needs with the direction/orientation with respect to the map. What's more, the odometry suffers drift over time, in which case the assumption of perfectly-known yaw information will gradually be problematic. While observing a circular LED without any asymmetry appearance cannot give orientation information. Therefore, it may have problems when long-term drifts occur. In this paper, we utilize a LiDAR scan matcher component that corrects the robot's orientation estimated with a raw odometry by matching LiDAR scan data with previous scans, then the cumulative error of the odometry can be compensated.

$$\theta_t = \gamma = \text{yaw}_{odom} + \text{yaw}_{LiDAR \rightarrow map} \quad (8)$$

Where  $\text{yaw}_{odom}$  is the raw orientation angle from the odometry, while  $\text{yaw}_{LiDAR \rightarrow map}$  is the included angle between the output TF of the LiDAR-SLAM (see Section III.B.b) and the map\_frame<sup>6</sup>.

### B. Multi-Sensor Fusion for VLP and SLAM

The proposed multi-sensor fusion for VLP-SLAM includes the building map and localization. To do so, firstly, VLP-constrained Gmapping is proposed to construct the occupancy grid map<sup>7</sup> based on the pre-build LED feature map. After that, we adopt the Adaptive Monte Carlo Localization (AMCL<sup>8</sup>) for LiDAR-SLAM to track the pose of the robot against the map from VLP-constrained Gmapping. Then an EKF-based pose estimation scheme is designed to stably obtain the global poses of the robot through predicting the pose from the odometry, and updating it by the AMCL and SLO-VLP observations. While the cumulative error from the odometry can be complemented by AMCL and SLO-VLP observation.

#### a) VLP-constrained Gmapping

LiDAR-SLAM method can be divided into two parts. The first part, creating occupancy grid map by obtaining the information from odometry and LiDAR scanning. The second part specifying the location of the robot on the created occupancy grid map using AMCL. In this section, we firstly proposed an improvement in Gmapping with VLP-constrained for mapping. Information about a prior-unknown environment is stored as a certainty grid map which is a two-dimensional array of identical units that keep their probability of being occupied by obstacle. Gmapping SLAM in its abstract concept is a problem of estimating the map  $m$  and the robot pose state  $\mathbf{s}_{1:t} = \mathbf{s}_1, \dots, \mathbf{s}_t$  given the motion odometry data  $u_{1:t-1} = u_1, \dots, u_{t-1}$  and the LiDAR scanning observation  $z_{1:t} = z_1, \dots, z_t$ . The RB particle

filter overcomes this issue by factorizing the posterior of the robot's trajectory and the map of the environment as below:

$$p(\mathbf{s}_{1:t}, m | z_{1:t}, u_{1:t-1}) = p(m | \mathbf{s}_{1:t}, z_{1:t}) \cdot p(\mathbf{s}_{1:t} | z_{1:t}, u_{1:t-1}) \quad (9)$$

Typically, Eq.9 can be decomposed into two steps. The odometry data and LiDAR sensor observation provide a solution for the RB particle filter to estimate the robot trajectory  $p(\mathbf{s}_{1:t} | z_{1:t}, u_{1:t-1})$ , after that, the posterior over maps  $p(m | \mathbf{s}_{1:t}, z_{1:t})$  can be computed analytically with robot trajectory  $\mathbf{s}_{1:t}$  and LiDAR observation  $z_{1:t}$  are known. The RB particle filter estimates the posterior probability robot trajectory  $p(\mathbf{s}_{1:t} | z_{1:t}, u_{1:t-1})$  by using particle filter, with each particle represents a potential trajectory (pose state) of the robot. Each particle sample is related to an individual map, the posterior  $p(\mathbf{s}_{1:t} | z_{1:t}, u_{1:t-1})$  is approximated with a set of particles with corresponding weights (importance factor). The weight of a particle is updated with a correspondence measure between a new scan and the map estimated by a scan matcher. Through the sampling-importance-resampling process, the continuous movement of the robot (trajectory) and the iteration of the particles cause the retention of high-weight particles and the discarding of low-weight particles. The steps of the RB particle filter algorithm are as follows:

- 1) Sampling: The prediction of next generation particles  $\{\mathbf{s}'_t^{(i)}\}$  is drawn from the previous generation  $\{\mathbf{s}_{t-1}^{(i)}\}$  by giving a prediction of the robot pose using the motion model (odometry)  $p(\mathbf{s}'_t^{(i)} | \mathbf{s}_{t-1}^{(i)}, u_{t-1})$ , where  $i$  denotes the index of the particle,  $\mathbf{s}'_t^{(i)}$  and  $\mathbf{s}_{t-1}^{(i)}$  are the predicted state of robot at the current moment and the previous moment respectively,  $u_{t-1}$  is the control parameter from the odometry.
- 2) Scan-Matching: After the sampling, these particles are improved by incorporating the current LiDAR scan-matching observations. Scan-matching is able to compute the best alignment between a reference map  $m_{t-1}^{(i)}$  and the current scan  $z_t$  give an odometry prediction  $\mathbf{s}'_t^{(i)}$ . A Gaussian approximation  $N(\mu_t^{(i)}, \Sigma_t^{(i)})$  [34] for each particle  $i$  is obtained for estimating the new poses (particles)  $\mathbf{s}_t^{(i)}$ .

$$\mathbf{s}_t^{(i)} = \arg\max p(\mathbf{s} | m_{t-1}^{(i)}, z_t, \mathbf{s}'_t^{(i)}) \quad (10)$$

- 3) Importance weighting: An individual importance weight  $w_t^{(i)}$  is assigned to each particle  $i$ , according to the importance sampling principle:

$$w_t^{(i)} = w_{t-1}^{(i)} \eta^{(i)} \quad (11)$$

Where,  $\eta^{(i)}$  is a normalization factor [34].

- 4) Adaptive resampling: During resampling, the particles with low importance weight  $w_t^{(i)}$  are typically replaced by samples with a high weight. An adaptive resampling threshold  $N_{eff}$ , which was set during the resampling process, indicates the degree of coincidence between the set particle and the robot trajectory.

$$N_{eff} = \frac{1}{\sum_i \frac{1}{\tilde{w}^{(i)2}}} \quad (12)$$

Where,  $\tilde{w}^{(i)}$  refers to the normalized weight of particle  $i$ .

- 5) Map estimation: For each particle, the corresponding map

<sup>4</sup> <https://wiki.ros.org/tf>

<sup>5</sup> <http://wiki.ros.org/navigation/Tutorials/RobotSetup/TF>

<sup>6</sup> <https://www.ros.org/rep/rep-0105.html>

<sup>7</sup> [https://en.wikipedia.org/wiki/Occupancy\\_grid\\_mapping](https://en.wikipedia.org/wiki/Occupancy_grid_mapping)

<sup>8</sup> <http://wiki.ros.org/amcl>

estimate  $p(m_t^{(i)} | s_{1:t}^{(i)}, z_{1:t})$  is computed based on the trajectory  $s_{1:t}^{(i)}$  of that sample (particle  $i$ ) and the history of observations  $z_{1:t}$ .

Gmapping based on RB particle filter, uses a relatively small number of particles to represent the SLAM posterior and reduces the computational effort required to perform resampling to successfully build very accurate maps. However, the SLAM map (occupancy grid map) belongs to the local map, which is based on the starting point of the SLAM Gmapping process (as origin). While the VLP estimation is global positioning, which is based on the prebuilt LED feature map, also called as VLP-map in this paper. The origin of the VLP-map is artificially defined, which is related to the ID coordinate of the LED luminaries. If the origin of the VLP-map and SLAM-map is not aligned, the integration between VLP and SLAM would be mismatched.

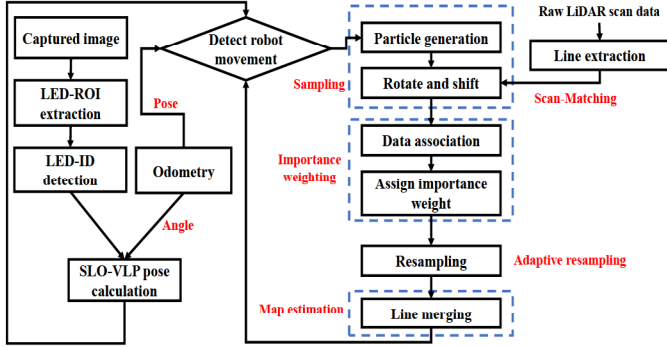


Fig.3 The architecture of the proposed VLP-constrained Gmapping

To overcome this problem, a VLP-constrained Gmapping method is proposed, shown in Fig.3, to ensure the alignment between the Gmapping built map and the VLP map. Since the obstacle or occupancy information detected in the SLAM-map is collected from LiDAR based on the current pose of the mobile robot. The SLO-VLP is adopted into the Gmapping as the initialization point, then the accuracy of mileage information from the odometry and LiDAR can be improved and constrained by fusing the SLO-VLP measurement data. The output SLAM-map would be associated with the LED beacons in the environment, so that the localization of LiDAR-SLAM can be integrated with the VLP measurement. It is worth to mention that, to some extent, the VLP-constrained Gmapping would not further refine the map building model. The purpose of this is to align the LiDAR-SLAM results with the VLP global map, so that the localization output of the LiDAR-SLAM can be integrated with the SLO-VLP.

#### b) Multi-Sensor Fusion based on EKF

For LiDAR-SLAM localization, AMCL is adapted to realize localization after the map building. AMCL is a probabilistic localization system for a robot moving in 2D, which uses a particle filter to track the pose of a robot against a known map with the LiDAR scanner match and odometry. Since the AMCL are not the contribution in this paper, we would not describe the details of it, to compensate the concept of AMCL, we refer readers to the book Probabilistic Robotics<sup>9</sup>. The full pipeline of the proposed multi-sensor for VLP-SLAM fusion based on EKF is illustrated in Fig4. Our goal is to estimate the full 3D ( $x$ ,  $y$ , and  $\theta$ ) pose of a mobile robot in 2D space, the state of the robot

at time  $t$  can be represented as a vector:

$$S_t = [x_t \ y_t \ \theta_t]^T \quad (13)$$

The EKF is adopted for state estimation of dynamic systems, which works as formulas (14) ~ (18). First, the current estimated state  $\hat{s}_t$  of the robot is predicted based on the previous state  $s_{t-1}$  with the state transition matrices  $F$ , and the control command  $u_t$ . For our application, the prediction step is based on the motion model of odometry measurements and the twist<sup>10</sup>. During the state prediction, the estimated error covariance,  $\hat{P}_t$ , is projected via  $F$ , and then perturbed by the process noise covariance  $Q_t$ .

$$\hat{s}_t = f(s_{t-1}, u_t) = F s_{t-1} + B u_t \quad (14)$$

$$\hat{P}_t = F P_{t-1} F^T + Q_t \quad (15)$$

The second step in the measurement update, the EKF incorporate the measurements  $z_t$  from the sensors, including the camera measurement for our SLO-VLP and the LiDAR scanning for AMCL, as input to correct its state estimation. The EKF gain  $K_t$  can be calculated by using the observation matrix  $H$  and the estimated error covariance  $\hat{P}_t$ :

$$K_t = \hat{P}_t H^T [H \hat{P}_t H^T + R_t]^{-1} \quad (16)$$

where,  $R_t$  is measurement noise covariance. Finally, the gain  $K_t$  is also used to update the state vector and covariance matrix:

$$s_t = \hat{s}_t + K_t (z_t - H \hat{s}_t) \quad (17)$$

$$P_t = (I - K_t H) \hat{P}_t \quad (18)$$

While the cumulative error or drift from the odometry can be estimated and compensated by the AMCL, since it can publish a *map\_frame* to *odom\_frame* transform, which essentially fixes the pose of the robot in the map frame.

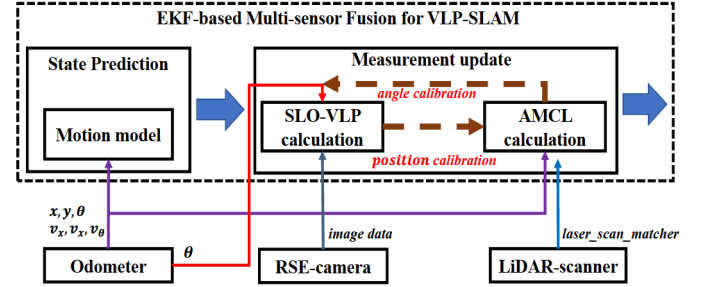


Fig.4 The pipeline of the proposed EKF-based VLP-SLAM

## IV. EVALUATION

In this section, we evaluate our system through real-world experiments, shown in Fig.5. We firstly evaluate the performance of the proposed VLP-constrained Gmapping, which show that our VLP-constrained Gmapping can drift or align the origin of the SLAM building map with the floorplan map. After that, we verify the property of the proposed multi-sensor fusion for VLP-SLAM, and show the strong performance and the robustness of our method compared with the state-of-the-art (SOTA) methods. Also, we embed the navigation function into our system to present the navigation and obstacle avoidance function, as an indication of the overall positioning and navigation performance. The video records of these demonstrations are available at the website:

- The alignment test between the floorplan map and the map built through the proposed VLP-constrained Gmapping: <https://www.bilibili.com/video/BV1av411a77b>
- Multi-sensor fusion for VLP-SLAM localization and navigation: <https://www.bilibili.com/video/BV1JX4y137Q7>

<sup>9</sup> <http://www.probabilistic-robotics.org/>

<sup>10</sup> <http://wiki.ros.org/navigation/Tutorials/RobotSetup/Odom>



- The robustness test when the LiDAR-SLAM is initialized incorrectly (VLP calibration for SLAM):  
<https://www.bilibili.com/video/BV1iA411N76g/>

#### A. Experimental settings

We setup a room-size (around  $12.0 \times 10.8 \text{ m}^2$ ) test field with 4 LEDs mounted on the yellow pole with 2.7 m high (see Fig.5 (a)). We use customized LEDs (our self-designed LED<sup>11</sup>) and robot for experiment, as shown by Fig.5 (b) and (c). The experiments are performed on a Raspberry Pi 3B mobile robot (Turtlebot 3 Burger<sup>12</sup> with Quad ARM Cortex-A53 Core 1.2 GHz Broadcom BCM2837 64 bits CPU and 1 GB RAM), which runs an Ubuntu Mate 16.04 OS equipped with a robot operating system (ROS<sup>13</sup>). The LEDs' radiation surface has a circular shape of size 17.5cm in diameter with power rating of around 18 W. We control the RSE camera sensor (MindVision UB-300) settings by

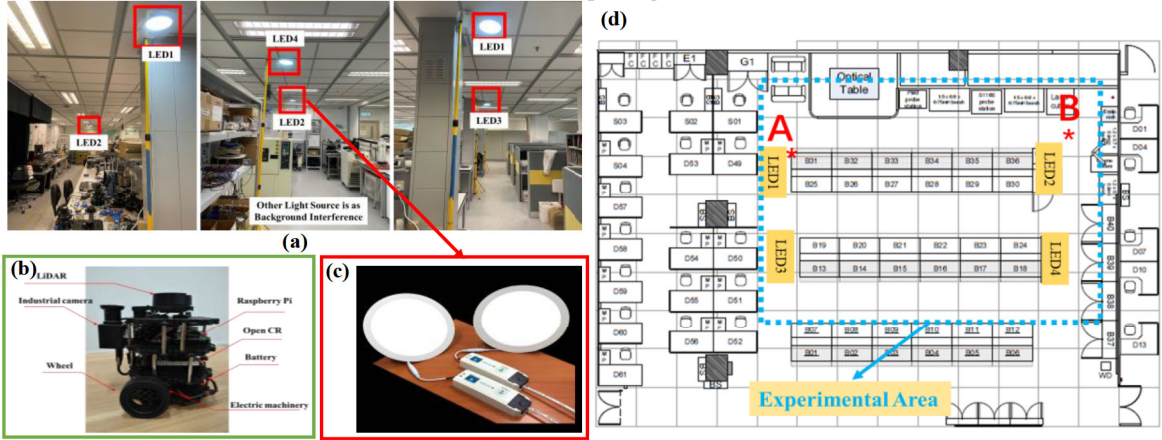


Fig.5 (a) Experimental platform; (b) The model of the robot; (c) Our self-produced LED; (d) The indoor map of our lab (A point is the origin of the prebuild LED feature map, B point is selected as a random point different from the origin).

#### B. Mapping performance

Mapping is the fundamental prerequisites for localization and navigation. In this section, we firstly study the map built by Gmapping. In continuation of our previous work [13], the prebuild LED feature map is fixed and predefined along with the floorplan (blueprint) map of the building. We setup the indoor grid map of our lab (Integrated Circuit Design Center, CYT-3010, HKUST), and modified it to the occupancy grid map so that it can be visualized in the RVIZ<sup>15</sup>. The map made from LiDAR-SLAM is a binary map (grid map) of navigable regions and boundary walls, which are represented through white and black (boundaries and obstacles) respectively for visualization purposes. The grid map for robot localization and navigation is a representation of aspect of interest (e.g., position of landmarks, obstacles) describing the environment in which the robot operates.

The origin of the map made by traditional Gmapping is the position of the robot at the beginning of the start-up, while the origin of the LED feature map is predefined and fixed (in this paper, we set it as the Point A in Fig.5 (d)). This means that, if the robot start building Gmapping at different position, then the origin of the SLAM-map is different, which makes mismatch between the localization output from LiDAR-SLAM and VLP.

minimizing the exposure time, so as to see clear strip patterns from the modulated LEDs. The image stream is captured at around 6 Hz with a  $2048 \times 1536$  resolution and recorded as ROS bags. The odometry and LiDAR (HLS-LFCD-LDS<sup>14</sup>, 2D laser scanner capable of sensing 360 degrees with one-degree angular resolution) is sampled at around 24 HZ and 5 HZ, respectively. Yet for these sensors, hardware synchronization is not available. Therefore, a multithreading loose synchronization framework is used in our algorithm. We run our algorithm on a laptop computer (Intel i7-10510U CPU @1.80 GHZ, Ubuntu 18.04) using the recorded bags from the robot. The major computation is done by the computer and physical components like the LiDAR sensors, RSE-camera, odometry, etc. are interfaced through the Raspberry Pi robot, which communicates serially with the computer through publishing or subscribing the message of the related ROS packages.

With the proposed VLP-constrained Gmapping process, the VLP-map and the generated SLAM map can be aligned, so that the fusion between VLP and LiDAR-SLAM is meaningful. It is worth to mention that, in this paper, we don't evaluate the map building accuracy, since the Gmapping is a related accurate map building method [38], [39]. The comparison of grid map made through the traditional Gmapping (beginning of Point A and Point B), and the proposed VLP-constrained Gmapping (beginning of Point B) are visualized in Fig.6, where we can see that, the resulting map has similar structure.

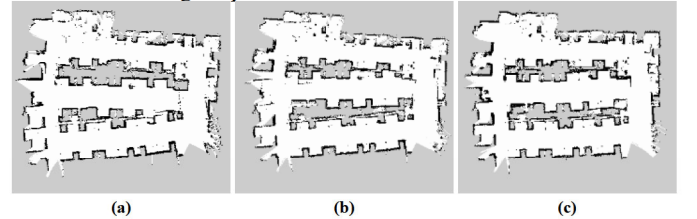


Fig.6 The resulting map through traditional Gmapping (a) start at Point A; and (b) start at Point B; (c) The resulting map through proposed VLP-constrained Gmapping start at Point B

Although the mapping performance among these three maps are similar, which fit the ground truth or the floorplan of our lab, the origin of the map is different. As can be seen in Fig.7, after the map building, we visualize the robot (stays at the same Point

<sup>11</sup> <http://liphio/hardware/>

<sup>12</sup> <https://emanual.robotis.com/docs/en/platform/turtlebot3/overview/>

<sup>13</sup> <https://www.ros.org/>

<sup>14</sup> [http://wiki.ros.org/hls\\_lfcd\\_lds\\_driver](http://wiki.ros.org/hls_lfcd_lds_driver)

<sup>15</sup> <http://wiki.ros.org/rviz>

B with same SLO-VLP calculation result) in RVIZ. However, the position of the robot in Fig7 (b) is pretty different from Fig7 (a) and (c), which is caused by the drift of the origin between the VLP-map and the SLAM-map.

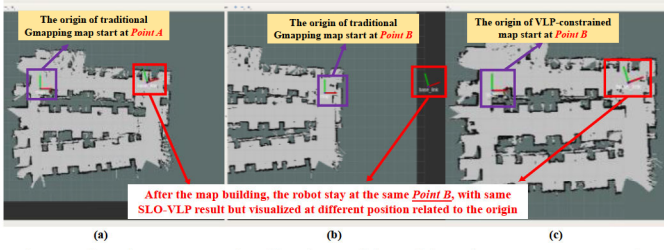


Fig. 7. Using the RVIZ to visualize the position of the robot (stay at same point B; “map” coordinate is the origin of the map; “base\_link” coordinate is the position of the robot through SLO-VLP calculation): (a) The SLAM-map made by traditional Gmapping start at Point A; (b) The SLAM-map made by traditional Gmapping start at Point B; (c) The SLAM-map made by proposed VLP-constrained Gmapping start at Point B

Without the VLP-constrained, the origin of the SLAM-map made from traditional Gmapping is the position of the robot at the beginning of the start-up, which may have a drift. For example, the robot starts at Point A, then the origin of the SLAM-map made from Gmapping is Point A, which is same as the origin of the LED feature map (also Point A). However, if the robot starts at Point B, then the origin of the SLAM-map made from Gmapping is Point B, which has a drift from Point A. As can be seen in Fig. 8, without the VLP-constrained, the SLAM-map made from Gmapping is term the start point (Point B) of the robot as the origin of the SLAM-map. While with the VLP-constrained Gmapping, the origin of the SLAM-map can be drifted to the same point as the origin (Point A) of the pre-build LED feature map.

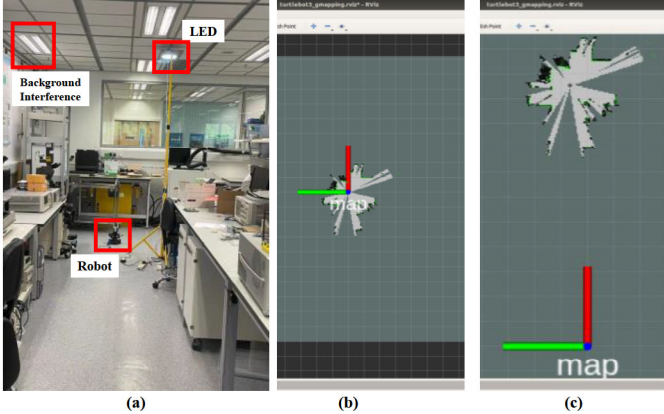


Fig. 8. The grip map made at the beginning of Point B; “map” coordinate is the origin of the map. (a) The test field; (b) Traditional Gmapping; (c) The proposed VLP-constrained Gmapping

The localization output of the SLAM is based on the origin of the SLAM-map, while the localization output of the SLO-VLP is based on the origin of the LED feature map, if the origin between these two maps is not aligned, the fusion between them would be mismatched. Therefore, our VLP-constrained Gmapping can align the LiDAR scan relative to the pre-build LED feature map. The origin of the VLP-constrained Gmapping map can be shifted to the origin of the LED feature map, so that it can realize the alignment between the localization output of LiDAR-SLAM and VLP.

### C. Localization performance

#### a) Positioning Accuracy

To evaluate the positioning accuracy of the proposed multi-sensor fusion for VLP-SLAM, two series of experiments were carried out. The first series are used to test the performance for motionless objects. 400 locations were randomly chosen in the experimental field to evaluate the positioning accuracy of the proposed multi-sensor fusion for VLP-SLAM. Without loss of generality, we also simultaneously calculate the positioning result from the SLO-VLP (400 samples) and the AMCL (50 samples) in the experiment. The result can be seen in Fig. 9. The average positioning accuracy of the proposed multi-sensor fusion for VLP-SLAM is 1.99 cm with the maximum error of 4.97cm, which is closed to that of SLO-VLP, which is 2.59 cm with maximum error of 5.72 cm (maintain similar level as our previous work [13]). While the average accuracy of the AMCL (LiDAR-SLAM) is 7.96 cm with maximum error of 12.98 cm.

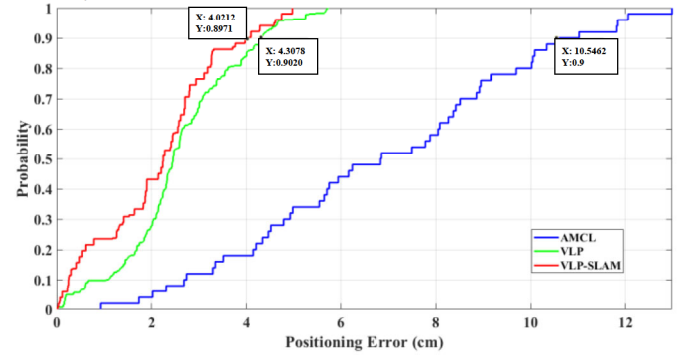


Fig. 9. CDF curve of the positioning error for the VLP-SLAM fusion, SLO-VLP, and AMCL

#### b) Robust and Real-time Pose Estimation

To further assess the real-time localization performance, we collected the data in trial to show the positioning performance among the SLO-VLP, AMCL, and our proposed VLP-SLAM during the movement of the robot. Fig. 10 shows the twice estimated trajectories, which travel around 46 m. The video demo for these two measurements is available in<sup>16</sup>. Due to the limitation of our hardware, we cannot provide the motion capture system to obtain the ground-truth of a moving robot, therefore, we do not discuss the accuracy for the dynamic localization. For the proposed VLP-SLAM method, on the one hand, the SLO-VLP can provide high accuracy position, which can not only used as the pose measurement for the robot but also can be used as the pose initialization for the AMCL. On the other hand, with the AMCL and the odometry, it still can provide localization when the LED is outage (no LED coverage can be). Besides, the cumulative error from the odometry can be corrected by the AMCL measurement.

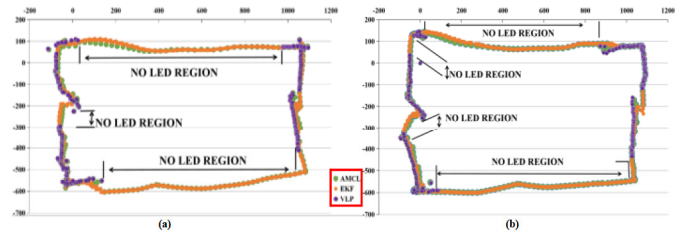


Fig. 10. The trajectory estimation of our multi-sensor fusion for VLP-SLAM method with SLO-VLP and AMCL. (a) Test One and (b) Test Two for similar path.

<sup>16</sup> Our Test Demo: <https://www.bilibili.com/video/BV1Zp4y1h7hF>



### c) Real-time Performance

Positioning speed is another key factor for localization systems. Especially, when the positioning terminal is moving, it can continuously receive information from the positioning system and calculate the current position in time. In this section, the computational time for position calculation of LiDAR-SLAM, SLO-VLP, and VLP-SLAM was continuously measured 300 times to calculate the average positioning time-consumption, as shown in Fig.11. The average computational time of our VLP-SLAM based on EKF is around 52ms. There are some special points of positioning time, which fluctuate from about 100 ms to 140 ms. These points are the EKF output when SLO-VLP or AMCL is available, otherwise, the mainly weight of the EKF output is calculated through the odometry sensor which is high frequency sampled. Please note that the odometry provided data at higher rates than the camera or LiDAR scanner. Even when the SLO-VLP is in-calculating (unavailable caused by calculation delay), the odometry prediction step of EKF is still used. Therefore, the derived pose estimates from VLP-SLAM can get smoothed temporally and can be sustained over a short time when LEDs are not available.

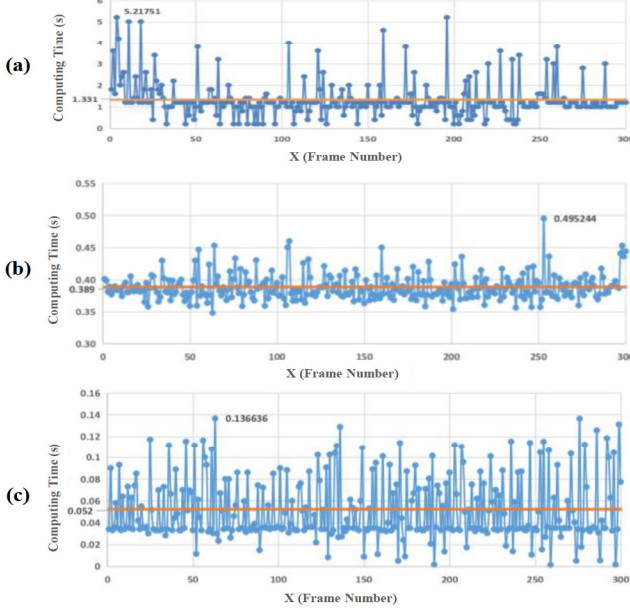


Fig.11. The measured positioning time (a) LiDAR-SLAM (AMCL); (b) SLO-VLP; (c) Multi-sensor fusion for VLP-SLAM

Note that we run the whole image process and data collection on a low-cost embedded platform Raspberry Pi 3B with a big size of captured image is 2048×1536 without any code optimization for ARM processors. After that the data (including the VLP observation, LiDAR scanning, and odometry data) are transmitted to the laptop which takes charge of multi-sensor fusion pose estimation and visualizes the result in RVIZ. The time cost here is the whole process covering both the image process and pose estimation (runtime in both laptop and the Raspberry), and also the time-cost of data transmission from robot to the laptop. Compare with the similar process platform with image size of 1640×1232 in Ref. [12], and 640×480 in Ref. [5] (Table I), the proposed multi-sensor fusion for VLP-SLAM is more efficient, and hence lightweight to be used on resource-constrained computational platform.

### D. Navigation performance

Once mapping and localization are successfully done, the navigation can be easily achieved. In this section, we embed our VLP-SLAM method into the Navigation Stack<sup>17</sup> in ROS to navigate the robot. While the map\_server<sup>18</sup> and AMCL part is the optional provided node, which are replaced by our proposed occupancy grid map based on VLP-constrained Gmapping and multi-sensor fusion for VLP-SLAM localization. The distributed ROS architecture of the navigation stack based on our VLP-SLAM is shown in Fig.12.

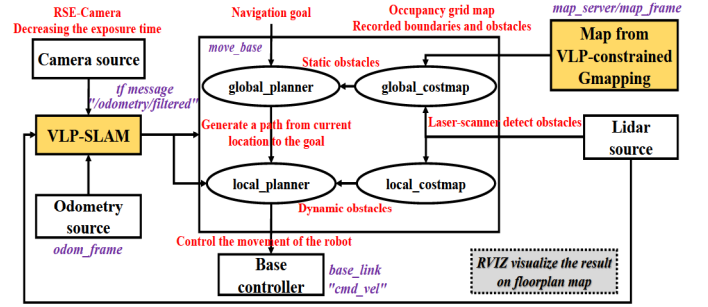


Fig.12. Visualization of the ROS computational graph for robot navigation based on our VLP-SLAM

The proposed navigation scheme uses our VLP-SLAM fusion method to estimate the pose of the robot, and the LiDAR for obstacle detection, the map data for path planning. ROS package move\_base<sup>19</sup> is adopted to accomplish autonomous navigation. This package uses the localization information from our multi-sensor fusion and provides move-commands to the mobile base of robot to move safely in the environment without colliding with obstacle. The framework also maintains two costmap<sup>20</sup> each for the local and global planner. The global planner is based on A Star search algorithm, while the local planner used the dynamic window approach [40]. Once a navigation goal is received, the global path planning algorithm takes charge of generating an appropriate path from the start pose to the target pose, while the local path planning is responsible for generating velocity commands based on the pose of the robot which is calculated through the our VLP-SLAM fusion. During the automatically navigation, the dynamic obstacles can be detected through the 2D LiDAR. Through the update of the local costmap to realize the dynamic obstacle avoidance. The accurate VLP pose estimation contributes to pose initialization for global path planning, while the real-time and robust VLP-SLAM pose estimation helps to local path planning. For the details about the navigation test, we strongly recommend the readers to our video demo:

- <https://www.bilibili.com/video/BV1JX4y137Q7>

### E. Discussion

In this section, we compare the performance of our VLP-SLAM with the SOTA works in the field of VLP in Table I. The average positioning accuracy, computing time, and the density of the LEDs in the related experimental platform are also reported objectively. It is obvious that the density of the LEDs in our VLP-SLAM system achieve state-of-the-art, with less latency (52ms) and high accuracy (2.0 cm). The proposed approach can work with sparse lighting distributions, which greatly increases the coverage of the effective positioning area. For a large area of (12.0×10.8×2.7 m<sup>3</sup>) only 4 LEDs are required to ensure high

<sup>17</sup> <http://wiki.ros.org/navigation/Tutorials/RobotSetup>

<sup>18</sup> [http://wiki.ros.org/map\\_server](http://wiki.ros.org/map_server)

<sup>19</sup> [http://wiki.ros.org/move\\_base](http://wiki.ros.org/move_base)

<sup>20</sup> [http://wiki.ros.org/costmap\\_2d](http://wiki.ros.org/costmap_2d)

accuracy positioning, while the other works cannot meet this high requirement. Compared to other sensor fusion approaches, our method perform favorably. Especially for the VLP-aided IMU method [5], [12]-[14], which suffers from bias or drift for long-term running. Our work can cope with the cumulative error through the LiDAR scan matching. Through the multi-sensor fusion, especially the LiDAR scanning compensation, the orientation angle from the odometry can perform well with considerable drifts after long-term experiment. So that the single LED VLP calculation, which is based on the orientation angle from the odometry, can obtain low-drift motion estimation. What's more, different harsh situations, such as without LED, background light interference, handover, etc., are included during our test. Therefore, the proposed multi-sensor fusion for VLP-SLAM can achieve well balance among accuracy, real-time performance, and robustness. The multi-sensor fusion can compensate the deficiencies of stand-alone sensors and provide more reliable, more robust positioning and navigation.

The LiDAR sensor make great contributions for the reliable localization and navigation. However, for LiDAR-SLAM, it is difficult to estimate the pose in the large space or long corridors without too much variety of observation. Since similar geometric regions in these environment may mislead the convergence of particles in AMCL. For example, the geometry of our indoor environment looks likely in region B19-B24 and B07-B12 (Fig.5d). When the robot is not under the VLP coverage area, the wrong initialization for LiDAR-SLAM would make the robot getting lost since the geometric region of these two parts is quite similar. However, when the VLP is available, the position of the robot can be calibrated to the right position. The evaluation about the VLP calibration for LiDAR-SLAM can be seen in the video demo<sup>21</sup>.

Besides, initialization is one of the crucial problems that needs to be solved in order to achieve fully autonomous navigation. For LiDAR-SLAM, the AMCL needs to initialize its filters, this is generally done with an initial pose message given by the user. In our VLP-SLAM method, the VLP can provide position initialization for the AMCL, while the AMCL can provide reliable orientation estimation for the SLO-VLP. Based on this, the robot is no longer need to head along fixed direction (e.g. X-axes) before running. Even if the manually initial pose (position and orientation) of the robot is not accurate, the LiDAR-SLAM can adjust the orientation of the robot, while the SLO-VLP can provide higher accuracy position estimation with the more correct orientation from the LiDAR. Meanwhile, the high position estimation from SLO-VLP can update overall pose estimation for the EKF, which can also act on the AMCL to improve the measurement from the AMCL. The interaction between VLP and LiDAR-SLAM provide reliable and accuracy pose estimation. The details about this can be visualized through the video demo<sup>22</sup>.

Admittedly, the proposed system still suffers a few limitations. The high accuracy VLP calculation is based on the accurate prebuild LED feature map. In other words, the actual installation position of the LED lamps is very important for the positioning accuracy. Especially, the automatic construction for the LED beacon in large scale scenarios. In future work, we would like to work on the tightly coupled VLP and SLAM through incorporating the LED markers into the maps and refining the SLAM map model simultaneously. On the one hand, it can generate the LED feature map with the occupancy grid map. On the other hand, the observation of external LED landmarks can be useful to deduce the trajectory drift and possibly correct the LiDAR-SLAM.

Table I. Performance comparison with the SOTA

Method	Average Accuracy (cm)	Time Cost (ms)	Require LEDs (at least)	Hardware	Dimension	Receiver Type	Density LEDs-Coverage ( $L \times W \times H$ )m <sup>3</sup>
R. [41]	14.0	N/A	3	STM32F103+computer	2D	PD+IMU	7 $-(1.5 \times 1.5 \times 2.5)$
R. [1]	3.9	44	2	Raspberry+computer	3D+yaw	Camera	9 $-(1.8 \times 1.8 \times 2.0)$
R. [11]	0.8	400	2	Raspberry+computer	3D+yaw	Camera	4 $-(1.0 \times 1.0 \times 1.5)$
R. [26]	17.5	N/A	1*	Smartphone	2D+3D	Camera	1 $-(3.0 \times 3.0 \times 2.0)$
R. [42]	3.2	43	1*	computer	3D+yaw	Camera	1 $-(0.8 \times 0.8 \times 2.0)$
R. [43]	2.3	60	1*	computer	2D+yaw	Camera	1 $-(1.8 \times 1.8 \times 3.0)$
R. [27]	5.5	N/A	1	Smartphone	6D	Camera+IMU	1 $-(2.7 \times 1.8 \times 1.5)$
R. [8]	13.4	N/A	1	Smartphone	3D+yaw	Camera+PDR	1 $-(1.0 \times 1.0 \times 2.6)$
R. [14]	5.0	N/A	1	Raspberry+computer	3D+yaw	Camera+IMU	23 $-(5.0 \times 4.0 \times 2.3)$
R. [12]	5.0	50	1	Raspberry+computer	3D+yaw	Camera+IMU	25 $-(5.0 \times 4.0 \times 2.3)$
R. [5]	3.0	78 <sup>#</sup>	1	Raspberry+computer	2D+yaw	Camera+encoder+gyroscope	4 $-(2.0 \times 2.0 \times 1.5)$
R. [5]	3.0	131.8 <sup>#</sup>	1	Raspberry+computer	2D+yaw	Camera+encoder+gyroscope	4 $-(2.0 \times 2.0 \times 1.5)$
R. [5]	2.2	81.5 <sup>#</sup>	1	Raspberry+computer	2D+yaw	Camera+encoder+gyroscope	4 $-(2.0 \times 2.0 \times 1.5)$
R. [13]	2.0	195	1	Raspberry+computer	3D+yaw	Camera+odom	3 $-(7.0 \times 3.8 \times 2.7)$
R. [13]	2.1	33	1 or 0	Raspberry+computer	3D+yaw	Camera+odom+IMU	3 $-(9.1 \times 4.0 \times 2.7)$
<b>Ours</b>	2.0	52	1 or 0	Raspberry+computer	3D+yaw	Camera+odom+LiDAR	4 $-(12.0 \times 10.8 \times 2.7)$

"\*" means that the LED lamp with beacon marker

"#" means that the position estimation was performed in post-processing, not real-time.

## V. CONCLUSION

In this paper, we pursue reliable, real-time, and accurate pose estimation for mobile robot through the multi-sensor fusion method based on EKF for VLP-SLAM. We relaxed the

assumption on the minimum number of concurrently observable LEDs from three to zero for the RSE-camera based VLP system through the fusion with odometry and LiDAR sensor. While the cumulative error of the odometry is compensated through the LiDAR scanning. We also embed our multi-sensor fusion for

<sup>21</sup> VLP calibration for SLAM:

<https://www.bilibili.com/video/BV1iA41N76g/>

<sup>22</sup> Pose initialization for VLP-SLAM:

<https://www.bilibili.com/video/BV1VX4y1G7wN>



VLP-SLAM into the navigation stack of ROS, owing to the high accuracy performance of our multi-sensor fusion scheme, the robot can move steadily according to the planned path to reach the designated location. The result shows that the our method has strong robustness with low latency (52ms) and high accuracy (2.0 cm), which can keep well balance among accuracy, real-time ability and coverage. In future work, we will deeply study the tightly coupled VLP and SLAM for incorporating the LED markers into the maps, which could construct the global map and optimize poses with sufficient features together with a method to model and reduce data uncertainty.

## VI. REFERENCES

- [1] P. Lin *et al*, "Real-time visible light positioning supporting fast moving speed," *Optics Express*, vol. 28, (10), pp. 14503-14510, 2020.
- [2] N. Huang *et al*, "Design and Demonstration of Robust Visible Light Positioning Based on Received Signal Strength," *J. Lightwave Technol.*, vol. 38, (20), pp. 5695-5707, 2020.
- [3] Y. Cai *et al*, "Indoor high precision three-dimensional positioning system based on visible light communication using particle swarm optimization," *IEEE Photonics Journal*, vol. 9, (6), pp. 1-20, 2017.
- [4] B. Chen *et al*, "Performance comparison and analysis on different optimization models for high-precision three-dimensional visible light positioning," *Optical Engineering*, vol. 57, (12), pp. 125101, 2018.
- [5] R. Amsters *et al*, "Visible Light Positioning Using Bayesian Filters," *J. Lightwave Technol.*, vol. 38, (21), pp. 5925-5936, 2020.
- [6] Y. Yang, J. Hao and J. Luo, "CeilingTalk: Lightweight indoor broadcast through LED-camera communication," *IEEE Transactions on Mobile Computing*, vol. 16, (12), pp. 3308-3319, 2017.
- [7] Y. Kuo *et al*, "Luxapose: Indoor positioning with mobile phones and visible light," in *Proceedings of the 20th Annual International Conference on Mobile Computing and Networking*, 2014, .
- [8] H. Huang *et al*, "Hybrid indoor localization scheme with image sensor-based visible light positioning and pedestrian dead reckoning," *Appl. Opt.*, vol. 58, (12), pp. 3214-3221, 2019.
- [9] A. Jovicic, "Qualcomm Lumicast: A high accuracy indoor positioning system based on visible light communication," *White Paper, Qualcomm, Apr*, 2016.
- [10] J. Fang *et al*, "High-speed indoor navigation system based on visible light and mobile phone," *IEEE Photonics Journal*, vol. 9, (2), pp. 1-11, 2017.
- [11] W. Guan *et al*, "High-Accuracy Robot Indoor Localization Scheme based on Robot Operating System using Visible Light Positioning," *IEEE Photonics Journal*, vol. 12, (2), pp. 1-16, 2020.
- [12] Q. Liang and M. Liu, "A tightly coupled VLC-inertial localization system by EKF," *IEEE Robotics and Automation Letters*, vol. 5, (2), pp. 3129-3136, 2020.
- [13] W. Guan *et al*, "Robust Robotic Localization using Visible Light Positioning and Inertial Fusion," *IEEE Sensors Journal*, pp. 1, 2021. . DOI: 10.1109/JSEN.2021.3053342.
- [14] Q. Liang, J. Lin and M. Liu, "Towards robust visible light positioning under LED shortage by visual-inertial fusion," in *2019 International Conference on Indoor Positioning and Indoor Navigation (IPIN)*, 2019, pp. 1-8.
- [15] S. Chen and W. Guan, "High Accuracy VLP based on Image Sensor using Error Calibration Method," *arXiv Preprint arXiv:2010.00529*, 2020.
- [16] T. Caselitz *et al*, "Monocular camera localization in 3d lidar maps," in *2016 IEEE/RSJ International Conference on Intelligent Robots and Systems (IROS)*, 2016, .
- [17] S. Chan, P. Wu and L. Fu, "Robust 2D indoor localization through laser SLAM and visual SLAM fusion," in *2018 IEEE International Conference on Systems, Man, and Cybernetics (SMC)*, 2018, .
- [18] V. Nguyen, A. Harati and R. Siegwart, "A lightweight SLAM algorithm using orthogonal planes for indoor mobile robotics," in *2007 IEEE/RSJ International Conference on Intelligent Robots and Systems*, 2007, .
- [19] P. Hu *et al*, "High speed LED-to-Camera communication using color shift keying with flicker mitigation," *IEEE Transactions on Mobile Computing*, 2019.
- [20] C. Xie *et al*, "The LED-ID detection and recognition method based on visible light positioning using proximity method," *IEEE Photonics Journal*, vol. 10, (2), pp. 1-16, 2018.
- [21] W. Guan *et al*, "Performance analysis and enhancement for visible light communication using CMOS sensors," *Opt. Commun.*, vol. 410, pp. 531-551, 2018.
- [22] Y. Xiao *et al*, "The Optical Bar Code Detection Method Based on Optical Camera Communication Using Discrete Fourier Transform," *IEEE Access*, vol. 8, pp. 123238-123252, 2020.
- [23] W. Guan *et al*, "High-precision indoor positioning algorithm based on visible light communication using complementary metal-oxide-semiconductor image sensor," *Optical Engineering*, vol. 58, (2), pp. 024101, 2019.
- [24] W. Guan *et al*, "High precision indoor visible light positioning algorithm based on double LEDs using CMOS image sensor," *Applied Sciences*, vol. 9, (6), pp. 1238, 2019.
- [25] H. Lee *et al*, "Rollinglight: Enabling line-of-sight light-to-camera communications," in *Proceedings of the 13th Annual International Conference on Mobile Systems, Applications, and Services*, 2015, .
- [26] R. Zhang *et al*, "A single LED positioning system based on circle projection," *IEEE Photonics Journal*, vol. 9, (4), pp. 1-9, 2017.
- [27] H. Cheng *et al*, "A Single LED Visible Light Positioning System Based on Geometric Features and CMOS Camera," *IEEE Photonics Technology Letters*, vol. 32, (17), pp. 1097-1100, 2020.
- [28] C. Cadena *et al*, "Past, present, and future of simultaneous localization and mapping: Toward the robust-perception age," *IEEE Transactions on Robotics*, vol. 32, (6), pp. 1309-1332, 2016.
- [29] H. Ye, Y. Chen and M. Liu, "Tightly coupled 3d lidar inertial odometry and mapping," in *2019 International Conference on Robotics and Automation (ICRA)*, 2019, pp. 3144-3150.
- [30] W. Hess *et al*, "Real-time loop closure in 2D LIDAR SLAM," in *2016 IEEE International Conference on Robotics and Automation (ICRA)*, 2016, .
- [31] B. Steux and O. El Hamzaoui, "tinySLAM: A SLAM algorithm in less than 200 lines C-language program," in *2010 11th International Conference on Control Automation Robotics & Vision*, 2010, .
- [32] M. Montemerlo *et al*, "FastSLAM: A factored solution to the simultaneous localization and mapping problem," *Aaai/Iaai*, vol. 593598, 2002.
- [33] S. Kohlbrecher *et al*, "Hector open source modules for autonomous mapping and navigation with rescue robots," in *Robot Soccer World Cup*, 2013, .
- [34] G. Grisetti, C. Stachniss and W. Burgard, "Improved techniques for grid mapping with rao-blackwellized particle filters," *IEEE Transactions on Robotics*, vol. 23, (1), pp. 34-46, 2007.
- [35] G. Grisetti, C. Stachniss and W. Burgard, "Improving grid-based slam with rao-blackwellized particle filters by adaptive proposals and selective resampling," in *Proceedings of the 2005 IEEE International Conference on Robotics and Automation*, 2005, .
- [36] W. Guan *et al*, "High-speed robust dynamic positioning and tracking method based on visual visible light communication using optical flow detection and Bayesian forecast," *IEEE Photonics Journal*, vol. 10, (3), pp. 1-22, 2018.
- [37] B. Hussain, C. Qiu and C. P. Yue, "A universal VLC modulator for retrofitting LED lighting and signage," in *2019 IEEE 8th Global Conference on Consumer Electronics (GCCE)*, 2019, .
- [38] J. M. Santos, D. Portugal and R. P. Rocha, "An evaluation of 2D SLAM techniques available in robot operating system," in *2013 IEEE International Symposium on Safety, Security, and Rescue Robotics (SSRR)*, 2013, .
- [39] K. Krinkin *et al*, "Evaluation of modern laser based indoor slam algorithms," in *2018 22nd Conference of Open Innovations Association (FRUCT)*, 2018, .
- [40] E. Marder-Eppstein *et al*, "The office marathon: Robust navigation in an indoor office environment," in *2010 IEEE International Conference on Robotics and Automation*, 2010, .
- [41] Z. Li *et al*, "Fusion of visible light indoor positioning and inertial navigation based on particle filter," *IEEE Photonics Journal*, vol. 9, (5), pp. 1-13, 2017.
- [42] W. Guan *et al*, "A novel three-dimensional indoor localization algorithm based on visual visible light communication using single LED," in *2018 IEEE International Conference on Automation, Electronics and Electrical Engineering (AUTEETEE)*, 2018, .
- [43] H. Li *et al*, "A Fast and High-accuracy Real-time Visible Light Positioning System based on Single LED Lamp with a Beacon," *Jphot*, pp. 1, 2020. Available: <https://ieeexplore.ieee.org/document/9233945>. DOI: 10.1109/JPHOT.2020.3032448.